Spatiotemporal structure of a laser beam over 144 km in a Canary Islands experiment

Alexandre S. Gurvich,[1] Michael E. Gorbunov,[1,*] Olga V. Fedorova,[1] Gottfried Kirchengast,[2] Veronika Proschek,[2] Gonzalo González Abad,[3] and Keith A. Tereszchuk[3]

[1]A. M. Obukhov Institute of Atmospheric Physics, Russian Academy of Sciences Pyzhevsky per. 3, Moscow 119017, Russia

[2]Wegener Center for Climate and Global Change and Institute for Geophysics, Astrophysics, and Meteorology/Institute of Physics, University of Graz Leechgasse 25, Graz A-8010, Austria

[3]Department of Chemistry, University of York, Heslington, York YO10 5DD, UK

*Corresponding author: m_e_gorbunov@mail.ru

Received 27 June 2012; accepted 17 August 2012;
posted 11 September 2012 (Doc. ID 171250); published 18 October 2012

We analyzed the observations of scintillations in a laser beam (532 nm, ~200 mW power) traveling along a 144 km path at an altitude of 2.2–2.4 km above sea level, just above the atmospheric boundary layer, between the islands of La Palma and Tenerife. The observations were performed during nighttime on 18 July 2011, by means of a telescope with an aperture diameter of 1 m. Strong scintillations were observed. The estimates of spatial spectra and correlation functions indicated that the observed intensity fields possess, statistically, a locally isotropic structure, which agrees with the idea of a locally isotropic turbulence. The estimates of spatial autospectra and autocorrelation functions of the intensity field indicated that the characteristic scale of the internal structure of the observed clusters is 6.5–8 mm, while the characteristic size of the clusters is 4–5 cm. The major contribution to the observed scintillations comes from the inhomogeneities of the intensity field with scales from 1–2 cm up to 10–12 cm. The analysis of the cross-spectra indicated that the hypothesis of frozen turbulence introduced by Taylor can be used for the description of spatiotemporal structure of intensity fluctuations of laser beams traveling through long paths in the atmosphere.

OCIS codes: 010.1300, 010.1330.

1. Introduction

Inhomogeneities of the atmospheric refractivity caused by turbulence destroy the spatial coherence of light propagating through the atmosphere. This phenomenon manifests itself, for example, in stellar scintillations that can be observed by the naked eye. In the optical range, the inhomogeneities responsible for scintillations, to a high degree of accuracy, are proportional to the temperature fluctuations of air. A model of the spatial structure of temperature fluctuations was developed by Obukhov and Corsin [1,2]. The Obukhov–Corsin model is based on the elaboration of the fundamental principles suggested by Kolmogorov for the description of developed, locally homogeneous turbulence. The spatial spectrum of the fluctuations that follows from this model is commonly referred to as the Kolmogorov spectrum.

The description of the temporal evolution of the temperature fluctuations at a fixed spatial point relies upon the hypothesis of the frozen turbulence introduced by J. Taylor [3] for the interpretation of measurements of turbulence in wind tunnels. Based on the fact that the air velocity fluctuations in such a tunnel are significantly smaller than the average velocity of the air flow, the hypothesis states that the statistics of turbulent fluctuations in the coordinate

1559-128X/12/307374-10$15.00/0

frame moving with the average velocity of the flow do not change with time.

In atmospheric turbulence, however, the relative fluctuations of the velocity are significantly larger than those in wind tunnels. In order to verify the applicability of the Taylor hypothesis to the atmosphere, a comparison was performed between the spectra of temperature fluctuations measured at a 70 m high tower and those obtained at an aircraft flying in the vicinity of the tower [4]. The wind velocity was 9 m/s, while the air speed of the aircraft was 55–88 m/s. The comparison corroborated the applicability of the hypothesis of frozen turbulence to a high accuracy. Furthermore, experimental studies of the spatiotemporal structure of fluctuations in the surface air [5] indicated that the evolution of inhomogeneities of air temperature and density, drifted by the wind, is small during the time of their displacement over a distance of the order of the scale of the inhomogeneities.

The hypothesis of frozen turbulence forms the basis of the description of the light intensity fluctuations caused by turbulence, as a function of time [6]. Diffraction effects in combination with the frozen turbulence hypothesis [6] explain, in particular, the "running shadows" at the input aperture of a telescope directed at a bright star. This was observed by astronomers as early as in the 17th century, when they removed the ocular and focused their eye on the aperture. In general, the validity of the hypothesis is undoubted for intensity fluctuations in a plane wave propagated through a thin layer of a turbulent medium. For narrow laser beams and large propagation distances, however, where the turbulent spread of the beam exceeds its diffractive divergence, its applicability is far from being that obvious. In a recent study [7], discussing the measurements of the fluctuations of a laser beam over a 149 km long atmospheric path, it was concluded that: "These results challenge the assumption of 'frozen' turbulence (Taylor hypothesis) commonly used in analyses."

Satellite-based observations of stars through the atmosphere in limb sounding geometry [8,9] indicate that the fluctuations of a laser beam along a limb path would become noticeable at perigee heights of 65–75 km. At perigee heights below 25–30 km, the fluctuations will be strong. For the description of strong fluctuations, the Markov approximation [10,11] was introduced. In this approximation, however, the equations that link the observed fluctuations with the atmospheric turbulence are still rather complicated. Their solutions have not yet been investigated sufficiently for the use of this approximation in computer-based modeling of the laser beam propagation along a limb path. A detailed experimental investigation is required to confirm the validity of this approximation.

One of the goals of an experimental campaign performed in the Canary Islands in July 2011, within the framework of a project on long-path greenhouse gas measurements [12] for basic demonstration of the new concept of infrared-laser occultation [13], was a better understanding of the spatiotemporal structure of intensity fluctuations caused by atmospheric turbulence within the observation plane after long-path laser beam propagation. A 144 km long optical path between the Northern Optical Telescope (NOT) observatory on La Palma and the Optical Ground Station (OGS) observatory on Tenerife was employed for the purpose [12]. A similar path has been used in an earlier study [14] of wave front fluctuations. The velocity of the transversal drift along this path with fixed transmitter and receiver locations is two to three orders of magnitude smaller than the satellite velocities in space-borne laser occultation [13]. Therefore, in order to best learn from the experimental results also for satellite observations, it was important to study the spatial spectra and correlation functions of the intensity and test the applicability of the Taylor hypothesis to the analysis of laser beam fluctuations. This study is discussed in this paper.

2. Observations of Intensity Fluctuations

The laser beam investigated in this study was emitted by a continuous wave, frequency-doubled, Nd:YAG laser (200 mW, 532 nm) located at the NOT observatory on La Palma (28.76° N, 17.89° W, 2392 m MSL altitude). The outgoing beam was collimated up to a diameter of 15 cm and directed with narrow beam divergence at the OGS telescope, located on Tenerife (28.30° N, 16.51° W, 2410 m MSL altitude), which has an aperture diameter of 1.016 m [12]. Within the OGS telescope optical assembly, the path distance to the coudé focus was 39 m. The optical path length between the transmitter and receiver was 144 km. The major part of the optical path was located above the ocean. The ray perigee height, taking the regular refraction into account, is about 2.2 km altitude. The ray path is, therefore, above the atmospheric boundary layer residing below 2 km altitude. In the absence of turbulence, due to diffraction effects only [15] and without intentional beam divergence, the beam size at the aperture of the OGS telescope would have a diameter of about 40 cm. The turbulent spread of the beam, however, significantly exceeded the diffractive divergence, and the diameter of the spot on the dome, where the telescope was mounted, significantly exceeded the aperture size due to the beam divergence [12]. Turbulence broke the beam into many separate clusters. Because of the vision inertia, the pattern of "running shadow" moving approximately in the horizontal direction could be observed with the naked eye. For a fast registration of the intensity field (I) of the received laser radiation, we employed a Prosilica GE-680 CCD camera mounted on an optical bench in the coudé focus room. The camera was equipped with a Fujinon HF75SA-1 lens with a focal length of 75 mm, which produced an image of the aperture of the OGS telescope onto the CCD matrix. The camera produced film records in the AVI format with a depth of 8 bits

per pixel at a frame rate of 205 frames per second. The dynamic range limitation determined by the bit depth resulted in a large number of under-/overexposed records that were rejected during the processing of the observations. The correction of the spectra distortion imposed by the finite exposure time is discussed below.

The observations were performed at nighttime in order to exclude any background scattered radiation from the sun. Figure 1 shows an example of the consecutive distributions of intensity $I(\boldsymbol{\rho},t)$ acquired from the aperture of the telescope using an acquisition time of about 5 ms, where $\boldsymbol{\rho}=(x,y)$ is the 2D vector of coordinates in the aperture plane, and t is the time.

It should be noted that the units of intensity are dimensionless throughout this paper. The images are vignetted by parts of the optical system assembly and limited by the visual field of the CCD camera lens. The dark spot in the middle of the image is the shadow of the secondary mirror, which has a diameter of 0.327 m. The knowledge of this diameter allows to transform the discrete coordinates of $\boldsymbol{\rho}$, initially specified by the pixel numbers, into the geometrical coordinates in the aperture plane.

The intensity field is broken into chaotic clusters whose positions change from frame to frame. Upon inspection of Fig. 1, however, one cannot see any noticeable ordered movement associated with "running shadows". Figure 2 shows an example of light flux $J(t)=\iint_S I(\boldsymbol{\rho},t)\mathrm{d}^2\boldsymbol{\rho}$ through the OGS aperture as a function of time. The observed fluctuations are primarily caused by the fluctuations of the atmospheric refractivity. Slow variations of attenuation from diffusion or absorption are negligible.

Despite significant spatial averaging over the aperture, which has a diameter of 1 m, the light flux indicates strong fluctuations with time. The ratio of the root mean square (rms) deviation $\sqrt{\overline{J^2}-\bar{J}^2}$ and the mean $\bar{J}$ estimated over the time interval of 120 s is 0.56. The probability distribution of J differs from the normal distribution because the light flux has short positive spikes. The fluctuations of $J(t)$ are caused by both turbulent displacements of the beam as a whole (beam wandering) and the beam spread.

Figure 3 shows the estimates of the mean intensity $\overline{I(\boldsymbol{\rho},t)}$ (left panel) in the telescope aperture and rms fluctuations of the intensity divided by the mean $\sqrt{\overline{I(\boldsymbol{\rho},t)^2}-\overline{I(\boldsymbol{\rho},t)}^2}/\overline{I(\boldsymbol{\rho},t)}$ (right panel). The mean values are evaluated from a representative sequence of 22,542 frames from the two records taken on 18 July 2011, within 00:05:46 to 00:08:23 [UTC + 1 h] (termed study time interval hereafter); the accumulation time was thus about 120 s. One pixel in the CCD matrix corresponds to $l_P=1.18$ mm in the aperture, which defines the Nyquist frequency of $\kappa_{\max}=\pi/l_P=2.65$ rad/mm. The white dashed circle indicates the border of the secondary mirror shadow. The coordinate axes are parallel to the sides of the CCD matrix. The white arrow indicates the horizontal direction. This rotation of the image is determined by the altitude-azimuth mounting of the OGS telescope. Throughout this paper, we will use the coordinate system rotated in such a way that the x axis is aligned horizontally. The shadows of the mounting rods of the secondary mirror are clearly visible. The temporal averaging damps the turbulent fluctuations in the intensity, and the measured estimates of its mean values indicate only insignificant fluctuations in comparison with the values of an individual measurement (i.e., a single recorded frame) shown in Fig. 1.

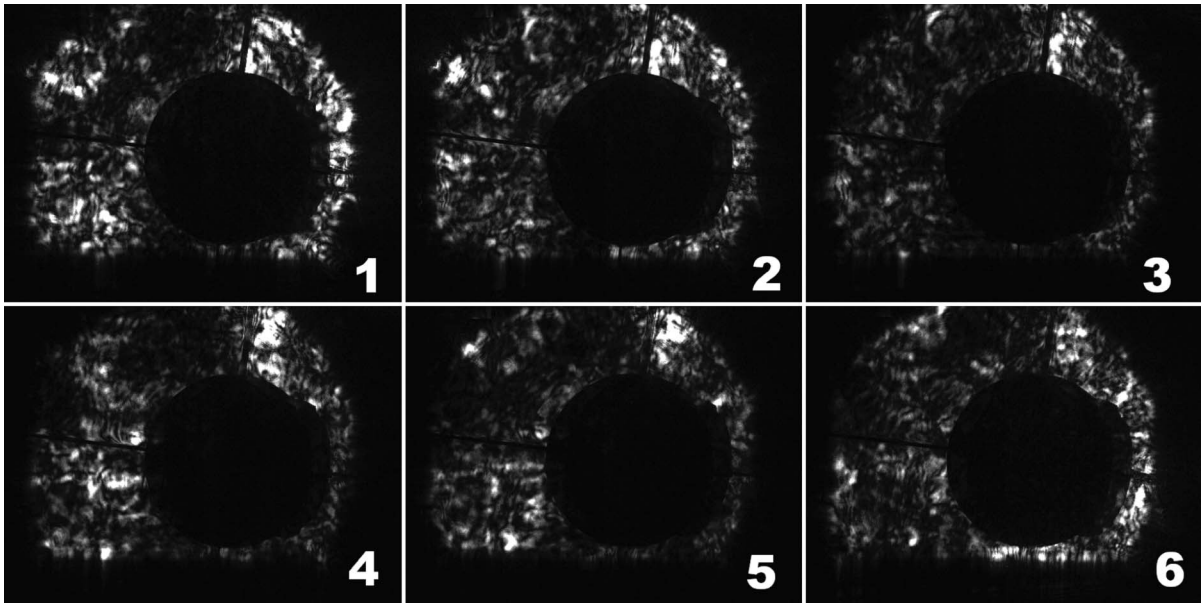

Fig. 1. Consecutive distributions of intensity $I(\boldsymbol{\rho};t)$, every about 5 ms, seen through the aperture of the OGS telescope. The distributions were observed on 18 July 2011 at 00:05:45 UTC + 1 h.

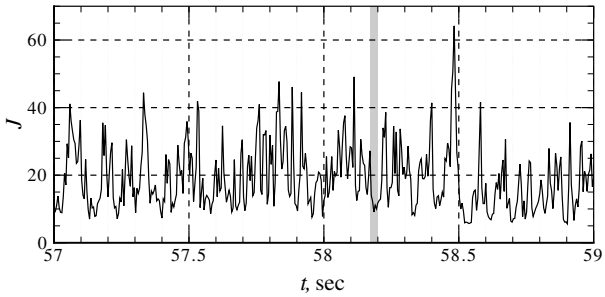

Fig. 2. Fragment of the record of light flux $J(t)$. The light-shaded area near 58.2 s indicates a 30 ms long interval corresponding to the six distributions $I(\boldsymbol{\rho}, t)$, shown in Fig. 1.

The ratio of the rms deviations and mean values in the right panel is mostly within a range of 1.5–1.7, except narrow bands around the edges and faulty areas of the CCD matrix due, most likely, to particles of dust on the surface of the matrix. Large rms variations are typical for strong scintillations [14,16–18].

In the left panel of Fig. 3, we selected three rectangular regions, 1, 2, and 3, respectively. For each rectangle, we estimated the mean and rms intensities over time, which were then averaged over all the rectangles. The ratio of the rms and the mean fluctuates within a range of 1.59–1.62, while the mean values have a range of 26.38–28.80. This allows for treating the observed fluctuations of the intensity in the approximation of a statistically homogeneous field using the concepts of mean values and spectral densities [19]. The sizes of $l_{x,y}$ along the x and y axes of the selected areas used for the analysis define the resolution $\Delta\kappa_{x,y} = 2\pi/l_{x,y}$ of the spatial spectrum.

3. Spectra and Correlation Functions of the Intensity Fluctuations in the Telescope Aperture

Observed distributions of intensity $I(\boldsymbol{\rho}; t)$ in the aperture of the OGS telescope are described by the following expression:

$$I(\boldsymbol{\rho}, t) = \frac{1}{2\tau}\int_{t-\tau}^{t+\tau} I^{(0)}(\boldsymbol{\rho}, t')\mathrm{d}t', \tag{1}$$

where $2\tau = 5$ ms is the exposure time and $I^{(0)}(\boldsymbol{\rho}, t)$ is the instant distribution of intensity in the aperture at a given time, t. We consider the intensities as measurements of a stationary, statistically homogeneous random field.

By substituting into Eq. (1) the expression of $I^{(0)}$ from the Fourier integral, we arrive at the following equation:

$$I^{(0)}(\boldsymbol{\rho}, t) = \int f^{(0)}(\boldsymbol{\kappa}, t)\exp(i\boldsymbol{\kappa}\boldsymbol{\rho})d^2\boldsymbol{\kappa}, \tag{2}$$

where $\boldsymbol{\kappa} = (\kappa_x, \kappa_y)$ is the wave vector, $f^{(0)}(\boldsymbol{\kappa}, t)$ is the Fourier transform of $I^{(0)}$, and t is the observation time. Employing Taylor's hypothesis for field, $I^{(0)}$, which states that $I^{(0)}(\boldsymbol{\rho}, t + \delta t) = I^{(0)}(\boldsymbol{\rho} - \boldsymbol{u}\delta t, t)$, and evaluating integral (1), we arrive at the following expression for $I(\boldsymbol{\rho}, t)$:

$$I(\boldsymbol{\rho}, t) = \int f^{(0)}(\boldsymbol{\kappa}, t)\mathrm{sinc}(\boldsymbol{\kappa}\boldsymbol{u}\tau)\exp(i(\boldsymbol{\kappa}\boldsymbol{\rho}))d^2\boldsymbol{\kappa},$$
$$\mathrm{sinc}(x) \equiv \frac{\sin(x)}{x}, \tag{3}$$

where $\boldsymbol{u}$ is the velocity vector of the drift of the inhomogeneities of $I^{(0)}$ in the aperture. From (3), it follows that the autospectrum [19] of the observed intensity field $I(\boldsymbol{\rho}, t)$ equals the following expression:

$$F^{(I)}(\boldsymbol{\kappa}, 0) = \langle(\mathrm{sinc}(\boldsymbol{\kappa}\boldsymbol{u}\tau))^2\rangle F^{(0)}(\boldsymbol{\kappa}, 0). \tag{4}$$

Velocity $\boldsymbol{u}$ is a random vector, and averaging in Eq. (4) is performed over an ensemble of measurements under the assumption that $\boldsymbol{u}$ and $f^{(0)}(\boldsymbol{\kappa}, t)$ are statistically independent.

Estimates of $F^{(I)}(\boldsymbol{\kappa}, 0)$ were evaluated for the three rectangular regions shown in the right-hand panel of Fig. 3. To this end, for each frame with number g (moment of time t_g) we evaluated, using the Hann window, the discrete Fourier transform $f^{(I)}(\boldsymbol{\kappa}, t_g)$ of the intensity $I(\boldsymbol{\rho}, t_g)$. Values of $|f^{(I)}(\boldsymbol{\kappa}, t_g)|^2$ were averaged over a series of frames. As a result, we obtained the following estimates of the autospectrum for each rectangle:

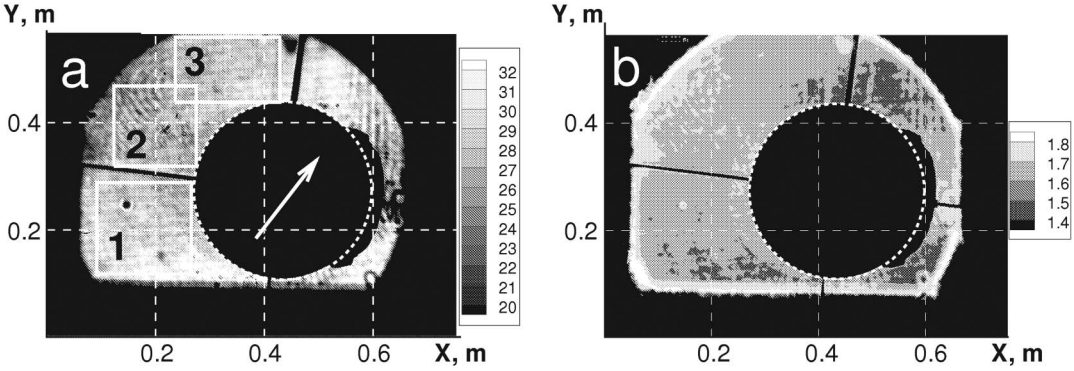

Fig. 3. Left: intensity distributions (dimensionless) in the aperture, averaged over the study time interval of 120 s. Right: distribution of the ratio of the rms and mean values.

$$F^{(I)}(\boldsymbol{\kappa},0)=\frac{1}{G}\sum_{g}|f^{(I)}(\boldsymbol{\kappa},t_g)|^2, \tag{5}$$

where G is the number of frames in the series. In these results, $G=22{,}542$. The autospectra were used to estimate the autocorrelation functions [19] $B^{(I)}(\delta\boldsymbol{\rho})=\langle I(\boldsymbol{\rho},t)I(\boldsymbol{\rho}+\delta\boldsymbol{\rho},t)\rangle$ of the intensity fluctuations in the telescope aperture:

$$B^{(I)}(\delta\boldsymbol{\rho})=\int F^{(I)}(\boldsymbol{\kappa},0)\exp(i\boldsymbol{\kappa}\delta\boldsymbol{\rho})d^2\boldsymbol{\kappa}. \tag{6}$$

In order to determine the applicability of the hypothesis of frozen turbulence for the analysis of scintillations, we considered the cross-spectral densities $F^{(I)}(\boldsymbol{\kappa};\delta t)$, $\delta t\neq 0$:

$$F^{(I)}(\boldsymbol{\kappa},\delta t)=\frac{1}{G}\sum_{g}f^{(I)}(\boldsymbol{\kappa},t_g)\bar{f}^{(I)}(\boldsymbol{\kappa},t_g+\delta t). \tag{7}$$

Here δt takes discrete values proportional to the acquisition time between frames.

The cross-spectral density is, generally speaking, a complex value being equal to $|F^{(I)}(\boldsymbol{\kappa},\delta t)|\exp(i\varphi^{(I)}(\boldsymbol{\kappa},\delta t))$, where $\varphi^{(I)}(\boldsymbol{\kappa},\delta t)$ is known as the phase spectrum, $-\pi\le\varphi^{(I)}<\pi$. The coherency spectrum $\mathrm{Coh}(\boldsymbol{\kappa},\delta t)$ is defined as follows:

$$\mathrm{Coh}(\boldsymbol{\kappa},\delta t)=\frac{|F^{(I)}(\boldsymbol{\kappa},\delta t)|}{F^{(I)}(\boldsymbol{\kappa},0)},\qquad 0\le\mathrm{Coh}\le 1. \tag{8}$$

If the hypothesis of frozen turbulence $I(\boldsymbol{\rho},t+\delta t)=I(\boldsymbol{\rho}-\boldsymbol{u}\delta t,t)$ holds for arbitrary $\boldsymbol{\rho}$ and t, the following equation must also hold:

$$F^{(I)}(\boldsymbol{\kappa},\delta t)=F^{(I)}(\boldsymbol{\kappa},0)\exp(i\varphi^{(I)}(\boldsymbol{\kappa},\delta t)). \tag{9}$$

In this case, the coherency spectrum is $\mathrm{Coh}(\boldsymbol{\kappa},\delta t)=1$, and the phase of the spectrum is $\varphi^{(I)}(\boldsymbol{\kappa},\delta t)=\delta t\boldsymbol{u}\boldsymbol{\kappa}$, a linear function of the wave number $\boldsymbol{\kappa}$. The deviation of $\mathrm{Coh}(\boldsymbol{\kappa},\delta t)$ from unity, as well as the violation of the linear dependency of $\varphi^{(I)}$ from the wave vector $\boldsymbol{\kappa}$ indicates the evolution of the intensity field clusters during their drift in the aperture plane.

4. Estimates of Spectra and Correlation Functions from Observations of Scintillations

Figure 4 presents the estimates of the 2D spectra of fluctuations, normalized to the dispersion, for the three rectangles shown in the left panel of Fig. 3. We estimated the dispersion of scintillations by using Parseval's formula:

$$\int\langle(I(\boldsymbol{\rho},t)-\langle I(\boldsymbol{\rho},t)\rangle)^2\rangle d^2\boldsymbol{\rho}=\frac{1}{4\pi^2}\int(F^{(I)}(\boldsymbol{\kappa},0))^2d^2\boldsymbol{\kappa}. \tag{10}$$

For wave numbers $\kappa>1.0-1.2$ rad/mm, the estimate of the power spectral density (PSD) is

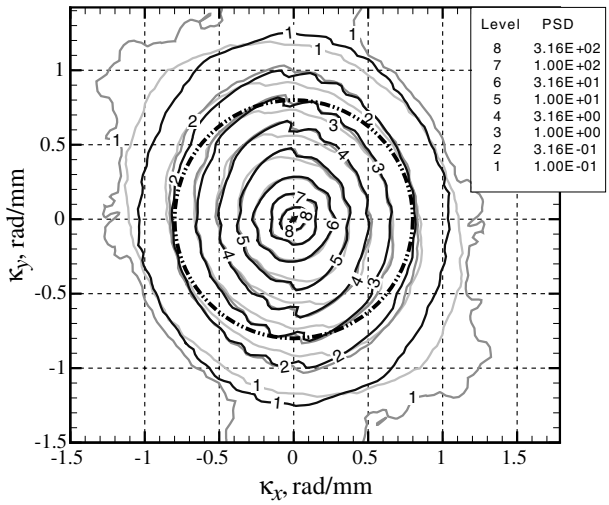

Fig. 4. Estimates of PSD [mm^4/rad^2] normalized for the dispersion of scintillations, observed during the study time interval. Light-gray isolines correspond to rectangle 1, gray ones to rectangle 2, black ones to rectangle 3. The radius of the circle shown by a bold black dash-dotted line equals 0.8 rad/mm. Isoline marks correspond to the level numbers in the legend.

unobtainable due to noise. The noise becomes noticeable for small values of PSD around 0.1. The isolines are circular in nature, slightly oblate in the direction of axis κ_x. For all three rectangles, the isolines are close to each other, while the PSD varies by three orders of magnitude. This corroborates the assumption of the statistical homogeneity of the intensity fluctuations in the telescope aperture plane.

Figure 5 shows the estimate of the normalized autocorrelation function $B^{(I)}(\delta\boldsymbol{\rho})/B^{(I)}(0)$ for rectangle 1. Autocorrelations for rectangles 2 and 3

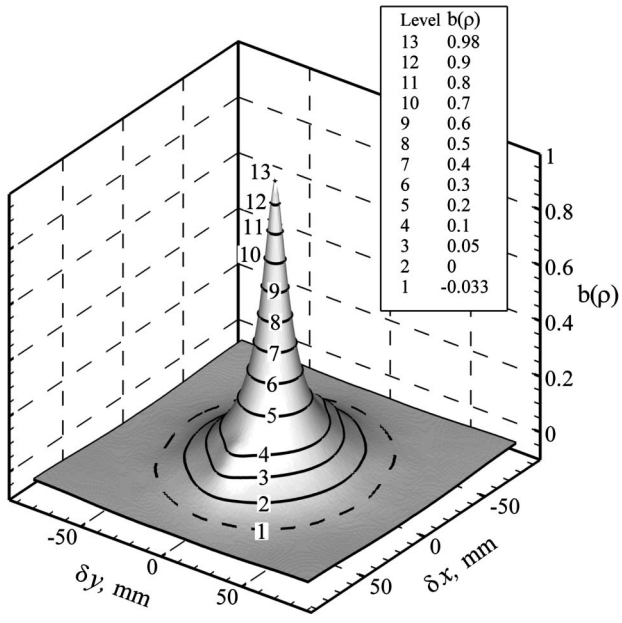

Fig. 5. Estimate of the normalized correlation function $B^{(I)}(\delta\boldsymbol{\rho})/B^{(I)}(0)$ for rectangle 1 during the study time interval. Isoline marks correspond to the level numbers in the legend.

(not shown) are practically indistinguishable from those for rectangle 1.

5. Discussion of Spectra and Correlation Functions

Atmospheric turbulence causes fluctuations in the intensity of a laser beam propagating through the atmosphere [6]. Because of local isotropy of turbulence, the 2D PSD isolines of the intensity field in the perpendicular cross-section are nearly circular. Observations along a near-surface path [20] indicated that turbulent fluctuations of density and temperature are isotropic. Those observations were performed with a wind velocity of several m/s, the exposure time in photographing the intensity field was $2\tau = 0.1$ ms, i.e., 50 times smaller than in the observations discussed in this paper. Therefore, the factor distorting the isotropy of the right-hand part of Eq. (4), which equals $\langle(\mathrm{sinc}(\boldsymbol{\kappa u}\tau))^2\rangle$, was close to unity [20].

The 2D PSD $F^{(I)}(\boldsymbol{\kappa}, 0)$ presented in Fig. 4 rapidly decreases in power with the increase of the wave number κ. The range of the variation of PSD is more than three orders of magnitude. To estimate the characteristic scale of the inhomogeneities making the major contribution to the dispersion of scintillation, we employed the fact that $F^{(I)}(\boldsymbol{\kappa}, 0)$ can be approximately represented as a function of $\kappa = \sqrt{\kappa_x^2 + \kappa_y^2}$. Changing to the polar coordinates in the wave number plane $\boldsymbol{\kappa}$ and integrating $F^{(I)}(\boldsymbol{\kappa}, 0)$ over the angular variable, we arrive at the following expression for the dispersion, σ_I^2:

$$\sigma_I^2 = \int F^{(I)}(\boldsymbol{\kappa}, 0) d^2\boldsymbol{\kappa} = 2\pi \int V^{(I)}(\kappa)\kappa^2 \mathrm{d}\ \ln\ \kappa, \qquad (11)$$

where

$$V^{(I)}(\kappa) = \frac{1}{2\pi}\int_0^{2\pi} F^{(I)}(\kappa\ \cos\ \varphi, \kappa\ \sin\ \varphi; 0)\mathrm{d}\varphi. \qquad (12)$$

Changing to the integration over $\ln\ \kappa$ allows for a detailed study of the contribution of small wave numbers in the dispersion. The dimensionless product $\kappa^2 V^{(I)}(\kappa)$ is the density of the contribution of the spectral component to the dispersion.

Figure 6 presents this density, $\kappa^2 V^{(I)}(\kappa)$, smoothed with a Gaussian window of width 0.004 rad/mm, as a scaled function of $\Lambda = 2\pi/\kappa$. The upper limit of the scale is defined by the sizes of the rectangles shown in Fig. 3. The area under the curves is proportional to the dispersion of scintillations. The maximum of dependence $\kappa^2 V^{(I)}(\kappa)$ corresponds to inhomogeneities with scales of about $\Lambda = 3 - 4$ cm. The major contribution to the dispersion of scintillations comes from clusters with scales from 1–2 to 10–12 cm. These are clearly visible in Fig. 1.

To estimate the scale of correlation of scintillation in the telescope aperture, we utilized the fact that the cross-sections of the surface $b(\delta\rho) = B^{(I)}(\delta\rho)/B^{(I)}(0)$, $\delta\rho = \sqrt{\delta x^2 + \delta y^2}$ by planes $B^{(I)}(\delta\rho) = \mathrm{const}$ are almost circular. Figure 7 presents functions $b(\delta\rho)$ for the three rectangles shown in Fig. 3.

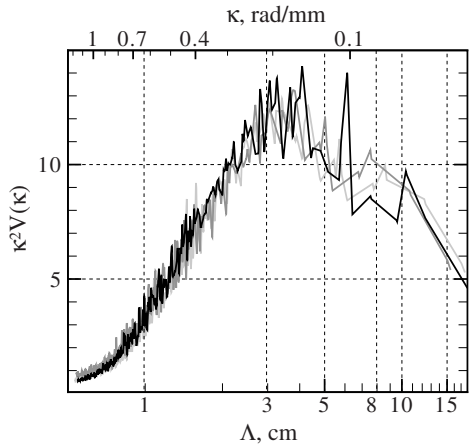

Fig. 6. Contribution of spectral components in the dispersion of scintillations as a scaled function of $\Lambda = 2\pi/\kappa$. The correspondence between shades of gray and rectangles is the same as in Fig. 4.

The correlation coefficient decreases down to 0.5 at $\delta\rho \approx 7$ cm, which provides an estimate of the characteristic internal scale of the intensity clusters. At a distance of $\delta\rho \approx 45 - 50$ cm, the correlation coefficient changes its sign, which provides an estimate of the characteristic external scale of the clusters. Because of the law of conservation of energy, the full integral of the correlation function $\int b(\delta\rho)\delta\rho^2 d\delta\rho$ must equal 0; therefore $b(\delta\rho)$ must be an alternating-sign function [6]. Turbulence results in a redistribution of the intensity in space, the formation of clusters must be accompanied by the appearance of low intensity areas, which is clearly visible in Fig. 1.

The 2D PSD $F^{(I)}(\boldsymbol{\kappa}, 0)$ shown in Fig. 4 and autocorrelation function $B^{(I)}(\delta\boldsymbol{\rho})/B^{(I)}(0)$ shown in Fig. 5 characterize the intensity fluctuations in space at an arbitrary moment of time, under the assumption of stationary scintillations. The coherence spectra shown in Fig. 8 describe the evolution of intensity clusters in time. Their comparison with autospectra ($\delta t = 0$) presented in Fig. 4 indicates that during the

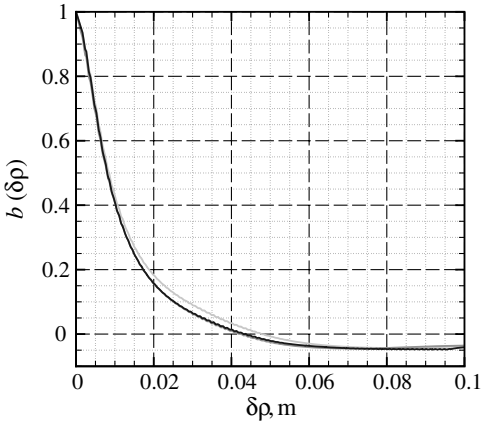

Fig. 7. Estimates of the correlation coefficient, $b(\delta\rho)$, of intensity fluctuations in the telescope aperture plane. The correspondence between shades of gray and rectangles is the same as in Fig. 4.

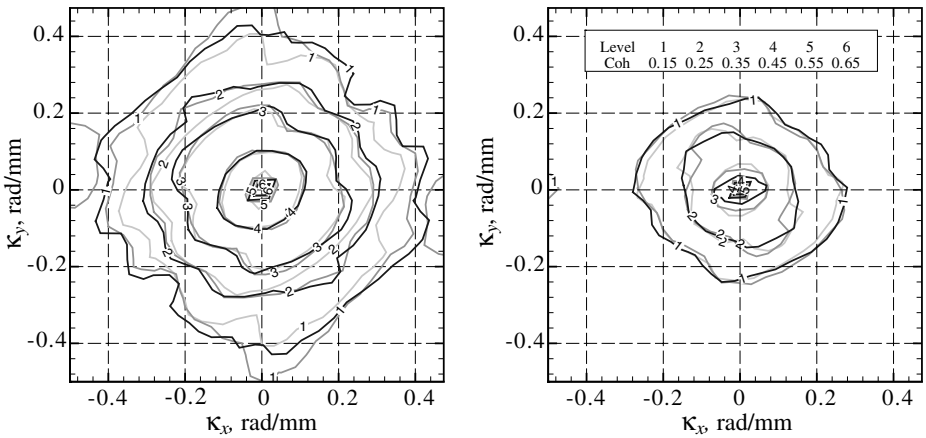

Fig. 8. Estimates of 2D coherence spectra $\mathrm{Coh}(\boldsymbol{\kappa};\delta t)$ defined by Eq. (8). Left panel: $\delta t = 5$ ms ($\mu = 1$); right panel: $\delta t = 10$ ms ($\mu = 2$). The correspondence between shades of gray and rectangles is the same as in Fig. 4.

time interval of 5 ms, the coherence spectrum significantly decreases, especially for large wave numbers $\kappa > 0.4$ rad mm^{-1}. Therefore, the correlation of intensity fluctuations decreases with time faster for smaller scale inhomogeneities of the intensity field. An intensity cluster in the telescope aperture plane not only drifts but also changes shape. This is noticeable when examining the distribution of intensity of individual frames, as presented in Fig. 1.

Figure 9 shows the 2D phase spectra. A comparison with Fig. 8 indicates that the phase spectrum can be estimated in the area of wave numbers (κ_x, κ_y) where the coherence spectrum is not too small. Outside this area, the uncertainty of the estimate of complex numbers $F^{(I)}(\boldsymbol{\kappa}, \delta t)$ [19] does not allow for a reliable estimate of their argument $\varphi(\boldsymbol{\kappa}, \delta t)$. Isolines here look like random trajectories. Because we defined the phase in the interval from $-\pi$ to π, its linear increase is equivalent to a saw-tooth function with jumps of 2π. Such jumps are observed at $\kappa_x = \pm 0.3$ rad mm^{-1} in the left panel and at $\kappa_x = \pm 0.15$ in the right panel. In order to better visualize the linear dependence of $\varphi(\boldsymbol{\kappa}, \delta t)$ from κ_x between the jumps, the phase spectra were averaged over κ_y in the region of $-0.425 \le \kappa_y \le 0.425$ rad mm^{-1}. The width of the region corresponds to an area where $F^{(I)}(\boldsymbol{\kappa}, \delta t)$ is large enough for $\delta t = 5$ ms. The resulting 1D phase spectra as functions of κ_x are presented in Fig. 10. The averaged phase of the cross-spectrum $F^{(I)}(\boldsymbol{\kappa}, \delta t)$ between the jumps fits closely a straight line. Therefore, during the time interval of $\delta t = 5$ ms, details of the field $I(\boldsymbol{\rho}, t)$ with scales of the order of 1 cm are seen with a large drift at a constant velocity u_0 in the aperture plane in the direction of the x axis at a distance of $u_0 \delta t$ without any significant change or deviation, in accordance to the hypothesis of frozen turbulence. The hypothesis holds better for smaller δt. Denoting the change of κ_x between the phase jumps as $\Delta\kappa_x$ we arrive at the following expression for the drift velocity: $u_0 = 2\pi/(\Delta\kappa_x \delta t)$. Substituting the values of $\Delta\kappa_x = 0.6$ rad mm^{-1} and $\delta t = 5$ ms, we obtain the estimate of $u_0 = 2.1$ m/s for the observations in our study time interval. The vector of $\mathbf{u}_0$ is directed along the Earth's surface: $u_0 = \{u_x, 0\}$.

For the intensity fluctuations in a plane wave with a constant wind velocity, the value of u_0 coincides

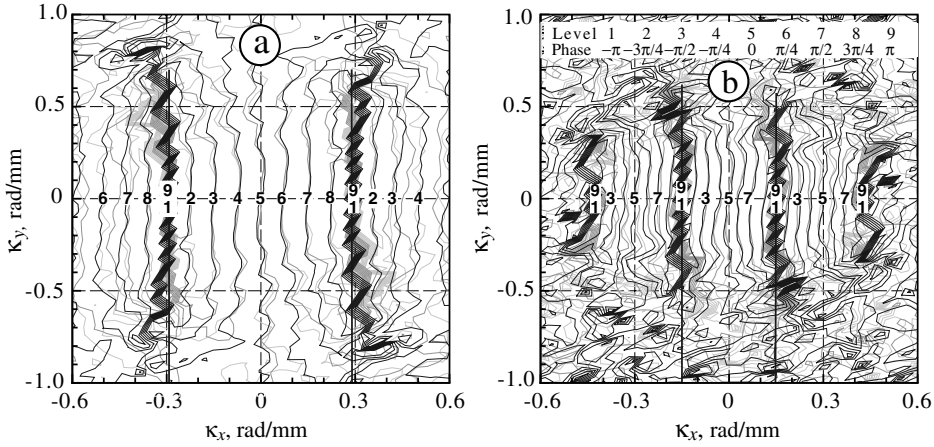

Fig. 9. Estimates of 2D phase spectra $\varphi(\boldsymbol{\kappa};\delta t)$. Left panel: $\delta t = 5$ ms ($\mu = 1$); right panel: $\delta t = 10$ ms ($\mu = 2$). The correspondence between shades of gray and rectangles is the same as in Fig. 4. Straight lines at $\kappa_x = \pm 0.3$ in the left panel and at $\kappa_x = \pm 0.15$ in the right-hand panel correspond to phase jumps of 2π.

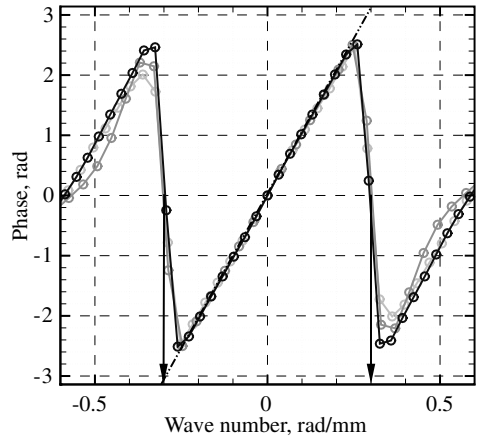

Fig. 10. Estimates of 1D phase spectra for $\delta t = 5$ ms evaluated for the three rectangles. The correspondence between shades of gray and rectangles is the same as in Fig. 4. The black dash-dotted line corresponds to $\bar{\varphi}(\kappa_x, \delta t) = u_0 \kappa_x \delta t$, where u_0 is the average drift velocity of the intensity clusters in the telescope aperture. The arrows mark the values of wave number $\kappa_x = \pm 0.3$ rad/mm, where the estimate of $\bar{\varphi}$ has a jump of 2π.

with the wind velocity component transverse to the direction of wave propagation [6]. In our observations, the estimated wind velocity along the propagation path, extracted from atmospheric analyses of the European Centre for Medium-Range Weather Forecasts (ECMWF), indicated significant variation both in its absolute value and direction (Fig. 11). The transverse component changes its sign. The scintillations are determined by the structural characteristic of turbulence C_n^2 [6]. The dependence of C_n^2 from the distance along the propagation path is, however, unknown. The evaluation of the weighting function that determines the relative contribution of turbulence in different sections of the ray path in the observed scintillations, under the condition of strong scintillations and a limited laser beam, is a challenge [11]. This makes it difficult to perform a quantitative comparison between the velocity of the "running shadows"

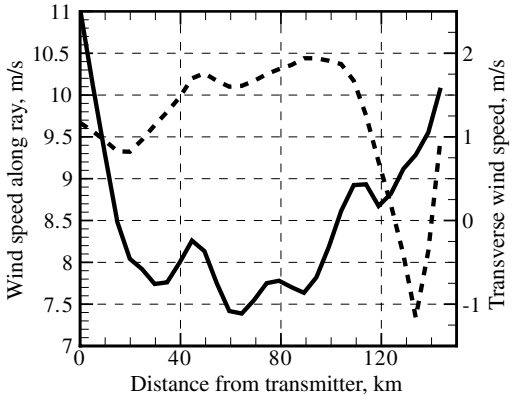

Fig. 11. Estimated wind speeds as a function of distance from the transmitter based on ECMWF analysis fields adjacent to the study time interval (18 July 2011, 00 UTC and 06 UTC analyses, linearly interpolated to the study time). Dashed line: along-beam component; solid line: transverse component.

and the transverse wind component. Notwithstanding, our estimate of the order of magnitude of u_0 is reasonably close to the independent information about the wind velocity along the propagation path.

A time span δt equal to 5 ms and 10 ms corresponds to a shift $u_0 \delta t$ of the clusters by 10 mm and 20 mm, respectively, which is comparable with the estimates of the characteristic external scales of the clusters inferred from the correlation function $b(\delta\rho)$ (Fig. 7). It follows from the coherence spectra (Fig. 8), for the shift $u_0 \delta t$ of 10 mm, that the correlation between values of the 2D PSD for wave number $\kappa = 0.1$ rad mm^{-1} is close to 0.5. The value of $\kappa = 0.1$ corresponds to a scale of $2\pi/0.1$ mm ≈ 63, which, by the order of magnitude, is close to the estimate of the characteristic size of a cluster. Therefore, clusters, when they drift by a distance of the order of their characteristic scale, are not destroyed. This was clearly noticeable also in visual observations of the "running shadows" on the dome of the OGS observatory.

Thus, Taylor's hypothesis holds for a spatiotemporal description of the intensity fluctuation field of a laser beam for observations through a turbulent medium at a large distance. A similarity between the evolution of the optical clusters and the evolution of temperature inhomogeneities in the atmosphere [5] is readily observed: Their lifetime roughly coincides with the time of their drift by a distance equal to their characteristic scale.

The estimate of velocity u_0 of the movement of intensity clusters in the telescope aperture was used for an estimate of the anisotropy of observed spectra (4) described by factor $\langle(\mathrm{sinc}(\boldsymbol{\kappa u}\tau))^2\rangle$. In our observations, the exposure time of the GE-680 camera can be assumed to be equal to $2\tau = 2$ ms. For $u_0 = 2.1$ m/s and $\kappa = 0.8$ rad/mm (Fig. 4), we infer that $0 \le |\tau \boldsymbol{u}_0 \boldsymbol{\kappa}| \le 0.17$ and $1 \ge (\mathrm{sinc}(\boldsymbol{\kappa u}_0 \tau))^2 \ge 0.35$. Therefore, the factor of $\langle(\mathrm{sinc}(\boldsymbol{\kappa u}\tau))^2\rangle$ must result in a greater oblateness of the isolines in the direction of the κ_x axis for larger values of κ_x.

To quantitatively estimate the influence of this factor arising at a finite exposure time, assume that the drift velocity of the clusters $\boldsymbol{u} = \tilde{\boldsymbol{u}} + \delta\boldsymbol{u}$, where $\tilde{\boldsymbol{u}}$ is the average drift velocity and $\delta\boldsymbol{u}$ is the velocity fluctuation, and $|\tilde{\boldsymbol{u}}| = u_0$. Let us also assume that the orthogonal components of the 2D vector $\delta\boldsymbol{u}$ are statistically independent and have a normal distribution with dispersion σ_u^2 and zero mean $\widetilde{\delta\boldsymbol{u}} = 0$. For the evaluation of $\langle(\mathrm{sinc}(\boldsymbol{\kappa u}\tau))^2\rangle$ we took $\sigma_u = 0.15 u_0$.

Figure 12 presents the 2D PSD of intensity $F^{(0)}(\boldsymbol{\kappa}; 0)$ in the telescope aperture obtained from the following formula:

$$F^{(0)}(\boldsymbol{\kappa}; 0) = F^{(I)}(\boldsymbol{\kappa}; 0) / \langle(\mathrm{sinc}(\boldsymbol{\kappa u}\tau))^2\rangle, \qquad (13)$$

which follows from Eq. (4).

It is noticeable that isoline shapes for $F^{(0)}(\boldsymbol{\kappa}; 0) > 1$ mm^4/rad^2 (for $\kappa < 0.8 - 0.9$ rad/mm) in Fig. 12 became closer to circles, compared to the ones in Fig. 4. This indicates that the notion of isotropy of the intensity fluctuation field in the telescope aperture for

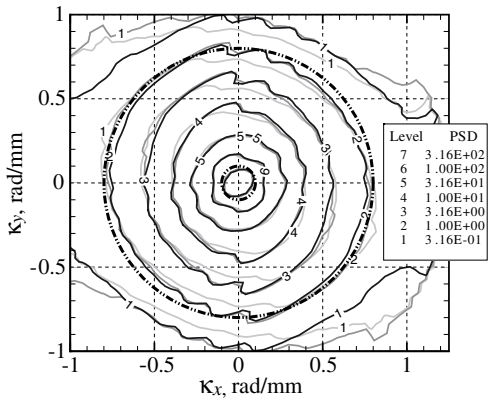

Fig. 12. 2D PSD $F^{(0)}(\boldsymbol{\kappa};0)$ obtained from the observations during the study time interval. The correspondance between shades of gray and rectanges is the same as in Fig. 4. The radii of the circles shown by the black dash-dotted lines equal 0.8 rad mm^{-1} and 0.1 rad mm^{-1}. Isoline marks correspond to the level numbers in the legend.

scales exceeding 6–7 mm agrees with the observations, consistent with previous work in the atmospheric surface layer [20]. The spectral components with larger wave numbers, corresponding to smaller scales, are interfered by the noise. Nevertheless, it is reasonable to assume the statistical isotropy of the scintillation field also for smaller scales or larger wave numbers. A noticeable anisotropy for very small wave numbers in Fig. 12 as well as in Fig. 4 relates to scales of 70–80 mm and more. These scales, however, correspond to the resolution limit of the spectral analysis. In this area, experimental estimates of PSD are therefore unreliable.

6. Conclusions

We analyzed the observations of scintillations in a laser beam (532 nm, ~200 mW power) traveling along a 144 km path at an altitude of 2.2–2.4 km above sea level, just above the atmospheric boundary layer, between the islands of La Palma and Tenerife. The observations were performed during nighttime on 18 July 2011. The observed intensity field of the laser beam in the telescope aperture with a diameter of 1 m at the end of the propagation path was broken by the turbulence into chaotic clusters.

The estimates of spatial spectra and correlation functions indicated that the observed intensity fields possess, statistically, a locally isotropic structure, which agrees with the idea of a locally isotropic turbulence. Rms intensity deviation divided by the mean intensity in the aperture is about 1.6, which signifies strong scintillations. The estimates of spatial auto-spectra and autocorrelation functions of the intensity field indicated that the characteristic scale of the internal structure of the observed clusters is 6.5–8 mm, while the characteristic size of the clusters is 4–5 cm. The major contribution to the observed scintillations comes from the inhomogeneities of the intensity field with scales from 1–2 cm up to 10–12 cm.

The analysis of the cross-spectra indicated that the hypothesis of frozen turbulence introduced by Taylor can be used for the description of spatiotemporal structure of intensity fluctuations of laser beams traveling through long paths in the atmosphere.

The authors are grateful to S. Schweitzer (Wegener Center, CityUniv. of Graz, Austria) for her complementary support to the scintillation observations as part of the July 2011 Canary Islands experiment. The research was funded by the European Space Agency's Support to Science Element (STSE) and supported by the Earth Observation Future Missions program, including ESA's OGS facility. ECMWF is acknowledged for access to its atmospheric analysis data.

References

1. A. M. Obukhov, "Structure of the temperature field in a turbulent flow," Izv. Akad. Nauk. SSSR Ser. Geogr. Geophys. **13**, 58–69 (1949).
2. S. Corrsin, "On the spectrum of isotropic temperature fluctuations in an isotropic turbulence," J. Appl. Phys. **22**, 469–473 (1951).
3. G. I. Taylor, "The spectrum of turbulence," Proc. R. Soc. Lond. Ser. A **164**, 476–490 (1938).
4. L. R. Tsvang, "Some characteristics of the spectra of temperature pulsations in the boundary layer of the atmosphere," Izv. Akad. Nauk. SSSR Ser. Geophys. **10**, 1594–1600 (1963).
5. A. S. Gurvich, "Influence of the temporal evolution of turbulent inhomogeneities on frequency spectra," Izv. Atmos. Ocean. Phys. **16**, 231–237 (1980).
6. V. I. Tatarskii, *The Effects of the Turbulent Atmosphere on Wave Propagation* (Keter, 1971).
7. M. A. Vorontsov, G. W. Carhart, V. S. Rao Gudimetla, T. Weyrauch, E. Stevenson, S. L. Lachinova, L. A. Beresnev, J. Liu, K. Rehder, and J. F. Riker, "Characterization of atmospheric turbulence effects over 149 km propagation path using multi-wavelength laser beacons," in *Proceedings of the 2010 AMOS Conference* (2010), p. E18.
8. A. S. Gurvich and V. Kan, "Structure of air density irregularities in the stratosphere from spacecraft observations of stellar scintillation: 1. Three-dimensional spectrum model and recovery of its parameters," Izv. Atmos. Ocean. Phys. **39**, 300–310 (2003).
9. V. F. Sofieva, A. S. Gurvich, F. Dalaudier, and V. Kan, "Reconstruction of internal gravity wave and turbulence parameters in the stratosphere using GOMOS scintillation measurements," J. Geophys. Res. **112**, D12113 (2007).
10. V. I. Tatarskii, "Shortwave propagation in a medium with random heterogeneities in approximate Markovian random process," Sov. Phys. JETP **29**, 1133–1138 (1969).
11. S. M. Rytov, Yu. A. Kravtsov, and V. I. Tatarskii, *Principles of Statistical Radiophysics, Vol. 3: Elements of Random Fields* (Springer-Verlag, 1987).
12. J. S. A. Brooke, P. F. Bernath, G. Kirchengast, C. B. Thomas, J.-G. Wang, K. A. Tereszchuk, G. González Abad, R. J. Hargreaves, C. A. Beale, J. J. Harrison, S. Schweitzer, V. Proschek, P. A. Martin, V. L. Kasyutich, C. Gerbig, O. Kolle, and A. Loescher, "Greenhouse gas measurements over a 144 km open path in the Canary Islands," Atmos. Meas. Tech. **5** (in press).
13. G. Kirchengast and S. Schweitzer, "Climate benchmark profiling of greenhouse gases and thermodynamic structure and wind from space," Geophys. Res. Lett. **38**, L13701 (2011).
14. N. Perlot, D. Giggenbach, H. Henniger, J. Horwath, M. Knapek, and K. Zettl, "Measurements of the beam-wave fluctuations over a 142 km atmospheric path," Proc. SPIE **6304**, 63041O (2006).

15. A. Ishimaru, "The beam wave case and remote sensing," in *Topics in Applied Physics* J. W. Strohbehn, ed. (Springer-Verlag, 1978), pp. 129–170.
16. M. E. Gracheva and A. S. Gurvich, "Strong fluctuations in the intensity of light propagated through the atmosphere close to the Earth," Radiophys. Quantum Electron. **8**, 511–515 (1965).
17. G. R. Ochs and R. S. Lawrence, "Saturation of laser-beam scintillation under conditions of strong atmospheric turbulence," J. Opt. Soc. Am. **59**, 226–227 (1969).
18. G. R. Ochs, R. R. Bergmtan, and J. R. Snyder, "Laser-beam scintillation over horizontal paths from 5.5 to 145 kilometers," J. Opt. Soc. Am. **59**, 231–234 (1969).
19. A. M. Yaglom, *Correlation Theory of Stationary and Related Random Functions* (Springer-Verlag, 1987), Vols. 1 and 2.
20. A. S. Gurvich, V. V. Pakhomov, and A. M. Cheremukhin, "The isotropy of refractive-index fluctuations of small-scale turbulence in the atmospheric surface layer," Izv. Atmos. Ocean. Phys. **7**, 49–52 (1971).